Inorg. Chem. **2006**, *45*, 1021−1031

Influence of Lattice Interactions on the Jahn−Teller Distortion of the $[Cu(H_2O)_6]^{2+}$ Ion: Dependence of the Crystal Structure of $K_2[Cu(H_2O)_6](SO_4)_{2x}(SeO_4)_{2-2x}$ upon the Sulfate/Selenate Ratio

Charles J. Simmons,*,† Horst Stratemeier,‡ Michael A. Hitchman,‡ and Mark J. Riley§

Division of Natural Sciences, University of Hawaii, Hilo, Hawaii 96720-4091, School of Chemistry, University of Tasmania, Box 252-75 Hobart, TAS 7001, Australia, and School of Molecular and Microbial Sciences, University of Queensland, St. Lucia, Queensland 4072, Australia

Received May 17, 2005

The temperature dependence of the structure of the mixed-anion Tutton salt $K_2[Cu(H_2O)_6](SO_4)_{2x}(SeO_4)_{2-2x}$ has been determined for crystals with 0, 17, 25, 68, 78, and 100% sulfate over the temperature range of 85−320 K. In every case, the $[Cu(H_2O)_6]^{2+}$ ion adopts a tetragonally elongated coordination geometry with an orthorhombic distortion. However, for the compounds with 0, 17, and 25% sulfate, the long and intermediate bonds occur on a different pair of water molecules from those with 68, 78, and 100% sulfate. A thermal equilibrium between the two forms is observed for each crystal, with this developing more readily as the proportions of the two counterions become more similar. Attempts to prepare a crystal with approximately equal amounts of sulfate and selenate were unsuccessful. The temperature dependence of the bond lengths has been analyzed using a model in which the Jahn−Teller potential surface of the $[Cu(H_2O)_6]^{2+}$ ion is perturbed by a lattice-strain interaction. The magnitude and sign of the orthorhombic component of this strain interaction depends on the proportion of sulfate to selenate. Significant deviations from Boltzmann statistics are observed for those crystals exhibiting a large temperature dependence of the average bond lengths, and this may be explained by cooperative interactions between neighboring complexes.

1. Introduction

The copper(II) Tutton salts of general formula $M_2[Cu(H_2O)_6](SO_4)_2$ provide good examples of the way in which the interplay of Jahn−Teller vibronic coupling and lattice forces decide the structure adopted by the $[Cu(H_2O)_6]^{2+}$ ion. The ammonium copper(II) Tutton salt is especially interesting in this respect because it exists in two distinct forms. When deuterated, it adopts a structure (form **A**) in which the long axis of the distorted $[Cu(D_2O)_6]^{2+}$ cation is directed toward the pair of O(8) water molecules,[1] whereas in the hydrogenous salt (form **B**), this direction is toward the O(7) waters.[2] This change is accompanied by slight alterations in the orientations and hydrogen-bonding interactions involving the ammonium and sulfate groups.[3] Application of pressure causes the deuterated compound to switch to form **B**,[3,4] the change exhibiting hysteresis when the pressure is decreased.[5,6] Both $(NH_4)_2[Cu(H_2O)_6](SO_4)_2$ and its deuterated analogue exhibit thermal equilibria between the two crystal forms.[1,7]

A question of particular interest is the cause of the structural change that accompanies deuteration. Recently, $(ND_4)_2[Cu(D_2O)_6](SO_4)_2$ was prepared in a metastable state in crystal modification **B**, and a highly accurate neutron

* To whom correspondence should be addressed. E-mail: simmonsc@hawaii.edu.
† University of Hawaii.
‡ University of Tasmania.
§ University of Queensland.

(1) Hathaway, B. J.; Hewat, A. W. *J. Solid State Chem.* **1984**, *51*, 364−375.
(2) Montgomery, H.; Lingafelter, E. *Acta Crystallogr.* **1966**, *20*, 659−662.
(3) Simmons, C. J.; Hitchman, M. A.; Stratemeier, H.; Schutz, A. J. *J. Am. Chem. Soc.* **1993**, *115*, 11304−11311.
(4) Rauw, W.; Ahsbas, H.; Hitchman, M. A.; Lukin, S.; Reinen, D.; Schultz, A. J.; Simmons, C. J.; Stratemeier, H. *Inorg. Chem.* **1996**, *35*, 1902−1911.
(5) Schultz, A. J.; Henning, R. W.; Hitchman, M. A.; Stratemeier, H. *Cryst. Growth Des.* **2003**, *3*, 403−407.
(6) Augustyniak, M. A.; Krupski, M. *Chem. Phys. Lett.* **1999**, *311*, 126−130.
(7) Hitchman, M. A.; Maaskant, W.; van der Plas, J.; Simmons, C. J.; Stratemeier, H. *J. Am. Chem. Soc.* **1999**, *121*, 1488−1501.

10.1021/ic050790j CCC: $33.50
Published on Web 01/05/2006

diffraction study found that the bond lengths and hydrogen-bond distances are very similar to those in the corresponding hydrogenous salt.[8] This implies that there is a very delicate balance between the two modifications, with the structural switch being associated with subtle differences in the hydrogen-bonding interactions, either involving the copper(II) complex or throughout the lattice as a whole.[3,8] A second point of interest concerns the thermal equilibria. Unlike most other copper(II) compounds exhibiting such behavior,[9,10] the proportions of the two forms differ significantly from Boltzmann statistics at higher temperatures.[7] In the original neutron diffraction analysis of the deuterated compound, the thermal equilibrium was attributed to the development of the rotational motion of the ammonium group.[1] In this context it should be noted that optical pumping of a vibrational mode associated with this rotational motion causes a structural switch for the partially deuterated compound.[11] Alternatively, it has been proposed that the anomalous thermal behavior is caused by cooperative interactions between the neighboring $[Cu(D_2O)_6]^{2+}$ complexes in the crystal lattice.[7]

To provide further information on these questions, a series of crystals with varying proportions of deuterium were studied by electron paramagnetic resonance (EPR) spectroscopy.[12] It was found that the structural switch occurred sharply at ~50% deuterium, with the thermal equilibrium of the compound containing 42% deuterium being similar to that of the pure hydrogenous compound. This line of investigation suggests that the study of other mixed crystals might be fruitful. As far as the disposition of the Cu−O bond lengths are concerned, the $K_2[Cu(H_2O)_6](SO_4)_2$ compound adopts form **A**.[4] The $Rb_2[Cu(H_2O)_6](SeO_4)_2$ compound also adopts this crystal modification, but the corresponding potassium salt exists in form **B**.[13] For the mixed-crystal series, $K_2[Cu(H_2O)_6](SO_4)_{2x}(SeO_4)_{2-2x}$ and $K_{2x}Rb_{2-2x}[Cu(H_2O)_6](SeO_4)_2$, it is therefore expected that a structural switch will occur as the proportion of sulfate to selenate is changed for the former series, and potassium to rubidium for the latter. It is hoped that the cause of the structural switch and the nature of any thermal equilibrium between the structural forms should be simpler to understand in these compounds as, unlike the ammonium group, the alkali metal ions do not participate in hydrogen-bonding interactions. The present paper describes the results obtained for the potassium sulfate/selenate mixed crystals.

2. Experimental Results

2.1. Preparation and Selection of Crystals. Samples of $K_2[Cu(H_2O)_6](SO_4)_2$ and $K_2[Cu(H_2O)_6](SeO_4)_2$ were prepared as described previously.[7,14] Crystals involving mixed anions were grown by recrystallizing mixtures of the pure salts with various ratios of sulfate to selenate in water. A crystal was selected from each batch, and the crystal structure was determined at room temperature. The ratio of sulfate to selenate was allowed to vary in the refinement of each structure, and it was found that this could be determined with an uncertainty of ~1%. Little correlation was found between the ratio of sulfate to selenate in each crystal and that in the batch of solids from which it was prepared. Unfortunately, despite the fact that numerous crystals were selected from the batch grown from a 50:50% mixture of sulfate/selenate, none was found to have a ratio approaching this. The structures of the crystals with a ratio approaching this most closely from both extremes, 25 and 68% sulfate, were studied over a range of temperatures, as were those of the pure compounds and two crystals with proportions between these limits, 17 and 78% sulfate.

2.2. X-ray Crystal Structure Determinations. Single crystals were ground to spheres of an approximate radius of 0.40 mm and mounted on glass capillaries. All X-ray diffraction data were collected using graphite monochromated Mo Kα radiation (λ = 0.71073 Å) on a Nonius Kappa CCD diffractometer fitted with an Oxford Model 700 Cryostream cooler at 85−320 K. Each data set was measured using a combination of φ and ω scans with κ offsets. The data frames were integrated and scaled using the Denzo-SMN package. The structures were solved by direct methods and refined by full-matrix least squares using the software teXsan for Windows version 1.06.

3. Results and Discussion

3.1. Crystal Structures. Details of the structure determinations for each crystal at 85−320 K are given in Supporting Information Table 1; atomic coordinates and thermal displacement parameters are available as Supporting Information. Cu−O distances and hydrogen-bonding interactions for each crystal at 85 and 320 K are given in Table 1, together with those reported previously for the pure compounds.

For the pure sulfate and selenate compounds, the Cu−O bond lengths agree with those of the less accurate previous determinations (Table 1). The $[Cu(H_2O)_6]^{2+}$ ion adopts a tetragonally elongated coordination geometry with a slight orthorhombic distortion in all the salts. However, although the bond lengths for the two pure compounds are quite similar, when the counterion is sulfate, the long and intermediate bonds are to O(8) and O(7), respectively, while the reverse is true for the selenate. As far as the disposition of the $[Cu(H_2O)_6]^{2+}$ ions, the sulfate thus adopts the structure observed for $(ND_4)_2[Cu(D_2O)_6](SO_4)_2$, designated form **A**, while the selenate adopts that of $(NH_4)_2[Cu(H_2O)_6](SO_4)_2$, form **B**. The arrangement of the $[Cu(H_2O)_6]^{2+}$ ions in the two compounds, viewed approximately perpendicular to the short Cu−O(9) bonds, is shown in Figure 1. It may be seen that the hydrogen-bonding interactions in the two compounds are very similar (see also Table 1).

Inspection of the Cu−O bond lengths for the series of compounds at ~320 K (Table 1) shows that the salts with 78 and 68% sulfate adopt form **A**, while those with 25 and 17% sulfate crystallize in form **B.** At ~85 K, the [Cu-

(8) Dobe, C.; Carver, G.; Bürgi, H.-B.; Treggenna-Piggott, P. L. W.; McIntyre, G. J.; Augustyniak-Jablokow, M. A.; Riley, M. J. *Inorg. Chem.* **2003**, *42*, 8524−8533.
(9) Hitchman, M. A. *Comments Inorg. Chem.* **1994**, *15*, 197−254.
(10) Falvello, L. R. *J. Chem. Soc., Dalton Trans.* **1997**, 4463−4475.
(11) Chen, Z.; Fei, S.; Strauss, H. L. *J. Am. Chem. Soc.* **1998**, *120*, 8789−8796.
(12) Henning, R. W.; Schultz, A. J.; Hitchman, M. A.; Kelly, G.; Astley, T. *Inorg. Chem.* **2000**, *39*, 765−769.
(13) Fleck, M.; Kolitsch, U. *Z. Kristallogr.* **2002**, *217*, 15−16.
(14) Whitnall, J.; Kennard, C. H. L.; Nimmo, J. K.; Moore, F. H. *Cryst. Struct. Commun.* **1975**, *4*, 709−712.

Table 1. Cu−O Bond Lengths and Hydrogen-Bonding Contacts for $K_2[Cu(H_2O)_6](SO_4)_{2x}(SeO_4)_{2-2x}$ Together with those Reported Previously for Pure Compounds

SO4 (%)	temp (K)	Cu−O(7) (Å)	Cu−O(8) (Å)	Cu−O(9) (Å)	hydrogen bonds (H···O) (Å)					
					O7−H15···O5	O7−H16···O6	O8−H17···O4	O8−H18···O6	O9−H19···O5	O9−H20···O3
100	320	2.0697(12)	2.2651(12)	1.9394(10)	2.0922	1.9613	1.8902	1.9793	1.9507	1.8436
	85	2.0287(6)	2.3122(6)	1.9422(6)	2.0034	1.8932	1.8519	1.9092	1.8579	1.8252
78	320	2.1085(15)	2.2269(17)	1.9410(14)	1.9410	1.9158	1.9009	2.0129	1.9270	1.8312
	85	2.0337(8)	2.3129(8)	1.9395(8)	2.0231	1.7931	1.8371	2.0042	1.7917	1.8375
68	320	2.1386(11)	2.1939(11)	1.9384(9)	2.1186	2.0837	1.9437	1.8622	1.8161	1.8782
	85	2.0313(7)	2.3105(8)	1.9407(8)	1.9760	1.8716	1.9337	2.0715	1.7183	1.8157
25	320	2.2556(18)	2.0774(15)	1.9353(15)	2.1553	2.1568	1.9828	2.0410	1.9779	2.0036
	85	2.3044(10)	2.0356(9)	1.9364(10)	2.2742	2.1555	1.9564	1.8871	1.8560	1.9213
17	320	2.275(2)	2.068(1)	1.940(2)	2.1862	1.9793	1.8977	2.0025	1.9360	1.7539
	85	2.3090(9)	2.0348(9)	1.9413(9)	2.2928	1.9274	2.0106	2.0639	2.1478	1.8498
0	320	2.2933(20)	2.0516(15)	1.940(19)	2.0619	2.0770	1.7391	1.9283	1.7801	1.8015
	85	2.316(1)	2.033(1)	1.9432(9)	2.2098	2.1264	1.9048	1.9867	2.0030	1.8794
0[a]	RT	2.297(2)	2.044(2)	1.936(2)	1.924	1.867	1.679	1.719	1.700	1.657
100[b]	RT	2.069(2)	2.278(2)	1.943(2)	1.775	1.813	1.733	1.805	1.697	1.680

[a] Whitnall, J.; Kennard, C. H. L.; Nimmo, J. K.; Moore, F. H. *Cryst. Struct. Commun.* **1975**, *4*, 709-712. [b] Robinson, D. J.; Kennard, C. H. L. *Cryst. Struct. Commun.* **1972**, *1*, 185-188.

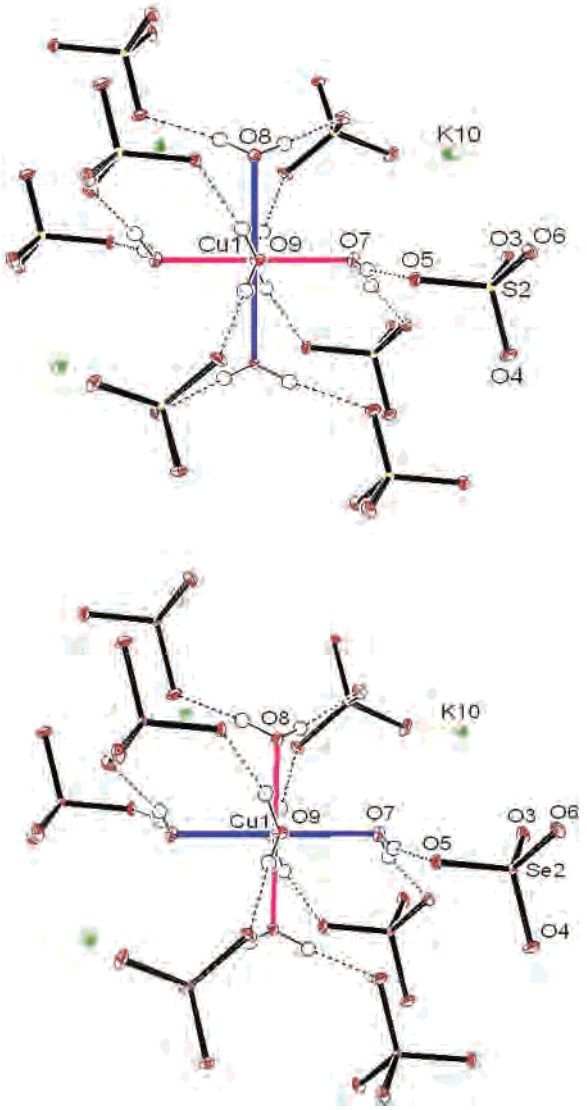

Figure 1. Coordination geometry and hydrogen-bonding interactions of $K_2[Cu(H_2O)_6](SO_4)_2$ (above) and $K_2[Cu(H_2O)_6](SeO_4)_2$ (below) viewed approximately perpendiular to the short Cu−O(9) direction.

$(H_2O)_6]^{2+}$ ions in crystals of all doping concentrations have similar bond lengths, although the directions of the two longer bonds differ in forms **A** and **B**. However, the two longer Cu−O bond lengths converge as the temperature is raised, the effect becoming more pronounced as the extent of the substitution increases and larger as sulfate is replaced by selenate in form **A** (Figure 2). It therefore seems that while the doped samples of $K_2[Cu(H_2O)_6](SO_4)_2$ and $K_2[Cu(H_2O)_6](SeO_4)_2$ basically adopt forms **A** and **B**, respectively, both exhibit a thermal equilibrium involving the other form.

3.2. Vibronic Coupling Model and Temperature Dependence of Cu−O Bond Lengths. Dynamic equilibria involving the direction of the Jahn−Teller distortion have been observed for many copper(II) complexes,[9,10] first being recognized as such by Silver and Getz in a pioneering study of the EPR spectrum of the $[Cu(H_2O)_6]^{2+}$ ion in Cu^{2+}-doped $K_2[Zn(H_2O)_6](SO_4)_2$.[15] In this approach, the SG model, it was shown that the temperature variation of the observed average *g* values of these copper(II) complexes could be interpreted satisfactorily in the presence of small strains by assuming a thermal equilibrium between two complexes identical in all respects except the interchange of the directions of the two higher *g* values. The basic assumption of the simple SG approach has been confirmed for several complexes,[16] including $(ND_4)_2[Cu(D_2O)_6](SO_4)_2$,[17] using the extended X-ray absorption fine structure (EXAFS) technique.

The so-called RHW vibronic coupling model was subsequently used to describe the temperature variation of the *g* values of Cu^{2+} doped into a range of Tutton salts by determining the vibronic wave functions and energy levels of the $[Cu(H_2O)_6]^{2+}$ complexes under the influence of both Jahn−Teller coupling and lattice strain interactions.[18,19] The RHW model has been extended to include the temperature dependence of the average metal−ligand bond lengths and

(15) Silver, B.; Getz, D. *J. Chem. Phys.* **1974**, *61*, 638−650.
(16) (a) Petrashen, V. E.; Yablokov, Yu. V.; Davidovitch, R. L. *Phys. Status Solidi B* **1980**, *101*, 117. (b) Ellis, P. J.; Freeman, H.; Hitchman, M. A.; Reinen, D.; Wagner, B. *Inorg. Chem.* **1994**, *33*, 1249−1250. (c) Masters, V. M.; Riley, M. J.; Hitchman, M. A. *J. Synchrotron Rad.* **1999**, *6*, 242−243.
(17) Masters, V. M.; Riley, M. J.; Hitchman, M. A. *Inorg. Chem.* **2001**, *40*, 843−849.
(18) Riley, M. J.; Hitchman, M. A.; wan Mohammed, A. *J. Chem. Phys.* **1987**, *87*, 3766−3778.
(19) Riley, M. J.; Hitchman, M. A.; Reinen, R. *Chem. Phys.* **1986**, *102*, 11−28.

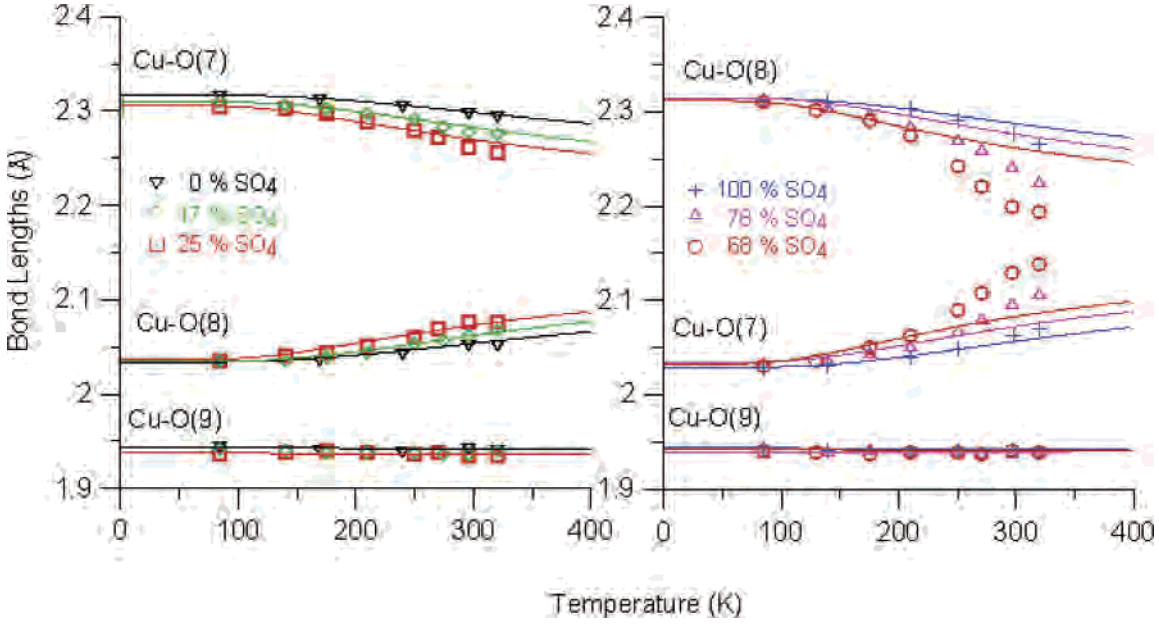

Figure 2. Temperature dependence of the Cu−O bond lengths. The curves show the dependence calculated using the RHW model using the parameters which gave optimum agreement with the experiment in the low-temperature region (see text for details).

thermal ellipsoid parameters observed in X-ray and neutron diffraction[20,21] and the situation when all three average g values change as a function of temperature.[22] The data for the present complexes were initially interpreted using the RHW model.

The deviation from a regular octahedral geometry of a complex distorted by $E_g \times e_g$ Jahn−Teller coupling is described in terms of the two components Q_θ and Q_ϵ of the Jahn−Teller active e_g vibration. The displacements and the corresponding composition of the electronic part of the ground-state wave function, Ψ_e, can also be expressed in terms of polar coordinates

$$Q_\theta = \rho \cos\phi \quad Q_\epsilon = \rho \sin\phi \tag{1a}$$

$$\Psi_e = d_{x^2-y^2} \cos(\phi/2) + d_{z^2} \sin(\phi/2) \tag{1b}$$

For a complex with six identical ligands, the distortion is driven by the linear coupling constant, A_1, and leads to the "Mexican hat" potential surface. At this level of approximation, the coupling to the Q_θ and Q_ϵ components of the e_g vibration is energetically equivalent, and the energy minimum is a circular well of radius ρ_o, in which the nuclear geometry fluctuates between various conformations of D_{4h} and D_{2h} symmetry that are generated by linear combinations of Q_θ and Q_ϵ. Higher-order coupling effects, represented by the parameter A_2, cause a "warping" of the Mexican hat potential surface to give three equivalent minima at $\phi = 0$, 120, and 240° for $A_2 > 0$ corresponding to tetragonal elongations with a $d_{x^2-y^2}$ type ground state and three saddle points at $\phi = 60$, 180, and 300° corresponding to tetragonal compressions. The extent of the warping is normally expressed by the parameter $\beta \approx A_2(A_1/h\nu_{JT})^2$, where $h\nu_{JT}$ is the energy of the Jahn−Teller active e_g vibrational mode; the energy difference between the minima and saddle points in the well is given by 2β.

In the low-symmetry environment of a Tutton salt crystal, the geometry of the complex is not determined solely by the JT effect but also by the strain imposed on it by the surrounding lattice, so that the three minima are no longer equal in energy. The general form of the "warped Mexican hat" potential energy can be parametrized using the first-order (A_1) and second-order (A_2) coupling constants, the wavenumber of the Jahn−Teller active e_g vibrational mode ($h\nu_{JT}$), as well as the strain imposed by the lattice (S_θ, S_ϵ). The approximation is made that the strain term does not destroy the symmetry of the cubic part of the Hamiltonian, so that there will be only one first-order and one second-order coupling constant and one harmonic vibrational force constant, instead of the six, nine, and two independent constants the low symmetry of the Tutton salt lattice actually requires.[18] The adiabatic potential energy surface is given by[20]

$$E^{\pm} = h\nu_{JT}(Q_\theta^2 + Q_\epsilon^2)/2 \pm [(A_1Q_\theta + A_2(Q_\theta^2 - Q_\epsilon^2) + S_\theta)^2 + (A_1Q_\epsilon - 2A_2Q_\theta Q_\epsilon + S_\epsilon)^2]^{1/2} \tag{2}$$

where the anharmonicity of the tetragonal component of the e_g vibration (Q_θ) has been neglected. The various parameters are conventionally given in units of cm^{-1}, except for the coordinates Q_θ and Q_ϵ, which are dimensionless.

To apply the RHW model to $K_2[Cu(H_2O)_6](SO_4)_{2x}(SeO_4)_{2-2x}$, the following calculations were made. (1) The vibronic wave functions and energy levels are determined by diagonalizing the vibronic Hamiltonian appropriate for the $E_g \times e_g$ coupling to second order, including strain and

(20) Bebendorf, J.; Bhrgi, H.-B.; Gamp, E.; Hitchman, M. A.; Murphy, A.; Reinen, D.; Riley, M. J.; Stratemeier, H. *Inorg. Chem.* **1996**, *35*, 7419−7429..
(21) Simmons, C. J.; Stratemeier, H.; Hanson, G. R.; Hitchman, M. A. *Inorg. Chem.* **2005**, *44*, 2753−2760.
(22) Hitchman, M. A.; Yablokov, Y. V.; Petrashen, V. E.; Augustyniak-Jablokow, M. A.; Stratemeier, H.; Riley, M. J.; Lukaszewicz, K.; Tomaszewski, P. E.; Pietrasko, A. *Inorg. Chem.* **2002**, *41*, 229−238.

Table 2. Optimum Parameters of Warped Mexican Hat Potentials for $[Cu(H_2O)_6]^{2+}$ Ions in Each Compound

% SO_4	A_1 (cm^{-1})	$h\nu_{JT}$ (cm^{-1})	β^a (cm^{-1})	S_θ (cm^{-1})	S_ϵ (cm^{-1})
100	950	262	347	-998	344
78	900	248	366	-1057	275
68	870	238	374	-1006	217
25	970	280	323	-1030	-284
17	980	281	320	-1018	-344
0	1000	292	304	-1033	-437

[a] $A_2(A_1/h\nu_{JT})^2$.

kinetic energy operators. The vibronic basis wave functions are products of two E_g ($\psi_\theta = d_{x^2-y^2}$ and $\psi_\epsilon = d_{z^2}$) metal orbital wave functions and the e_g vibration, which is taken as an expansion of two one-dimensional harmonic oscillator basis functions. (In the present calculations, harmonic oscillator basis functions, $n_v = 0, ..., 32$, are used which gives a total vibronic basis of 1122 (i.e., $2(1/2)(n_v + 1)(n_v + 2)$).) (2) The expectation values for $\langle Q_\theta\rangle_i$ and $\langle Q_\epsilon\rangle_i$ of each level are calculated from the vibronic wave functions found in step 1. (3) The Cu−O bond lengths associated with each vibronic level, $\langle d(\text{Cu}-\text{O})\rangle_i$, are calculated via the relationships between the dimensionless $\langle Q_\theta\rangle_i$ and $\langle Q_\epsilon\rangle_i$ coordinates and the mass- and energy-weighted ligand displacements $\langle x\rangle_i$, $\langle y\rangle_i$, and $\langle z\rangle_i$[17,20]

$$\langle x\rangle_i = -(1/\sqrt{12})\langle Q_\theta\rangle_i + (1/2)\langle Q_\epsilon\rangle_i \quad (3a)$$

$$\langle y\rangle_i = -(1/\sqrt{12})\langle Q_\theta\rangle_i - (1/2)\langle Q_\epsilon\rangle_i \quad (3b)$$

$$\langle z\rangle_i = (1/\sqrt{3})\langle Q_\theta\rangle_i \quad (3c)$$

where $\langle x\rangle_i$, $\langle y\rangle_i$, and $\langle z\rangle_i$ are the displacements relative to the undistorted octahedral geometry directed along the bonds. The mass- and energy-weighted displacements may be transformed into absolute displacements, $d_{x,i}$, etc., according to eq 4[20]

$$d_{x,i}\,(\text{Å}) = 5.8065\langle x\rangle_i(Mh\nu_{JT})^{-1/2} \quad (4)$$

(4) The calculated Cu−O bond lengths and energies of all vibronic levels, i, are then used to calculate the overall Boltzmann weighted averaged Cu−O bond lengths

$$d(\text{Cu}-\text{O})_{calcd} = \sum_i Z\exp(-\epsilon_i/kT)\langle d(\text{Cu}-\text{O})\rangle_i \quad (5)$$

where

$$Z = \sum_i \exp(-\epsilon_i/kT)$$

The values of the parameters describing the JT coupling ($h\nu_{JT}$, A_1, A_2) and the influence of the lattice strain (S_θ, S_ϵ) are optimized by minimizing the differences between the calculated and observed Cu−O bond lengths, especially at low temperature. A similar analysis can be made for the mean-squared displacements, $\langle d(\text{Cu}-\text{O})^2\rangle$.[17]

The resulting optimized parameters for each compound are given in Table 2. Notice that comparatively little variation occurs and that the average estimates, $A_1 = 945$ cm^{-1}, $h\nu_{JT} = 267$ cm^{-1}, and $\beta = 339$ cm^{-1} ($A_2 \approx 27$ cm^{-1}), are broadly similar to those reported previously for the $[Cu(H_2O)_6]^{2+}$ ion. For example, a value of $A_1 = 900$ cm^{-1} was found in a study of the EPR spectra of Cu^{2+}-doped zinc(II) Tutton salts,[18] and in a study of the temperature dependence of the Cr−O bond lengths of $(ND_4)_2[Cr(D_2O)_6](SO_4)_2$,[23] a value of 1100 cm^{-1} was used to fit the temperature dependence of Cu−O bond lengths in an EXAFS study of $(ND_4)_2[Cu(D_2O)_6](SO_4)_2$,[17] while an average estimate of 960 cm^{-1} was reported by Bill[24] for a range of copper(II) oxygen complexes. The present energy of the Jahn−Teller active vibration, ~267 cm^{-1}, is lower than that used in the previous analyses of the EPR spectra of the $[Cu(H_2O)_6]^{2+}$ ion, 300 cm^{-1},[18] and is slightly lower than the average value of 285 cm^{-1} observed for a series of nickel(II) and zinc(II) hexahydrated ions in different lattices,[25] but it is very similar to the value (254 cm^{-1}) used for the analysis of Cr−O bond lengths for $(ND_4)_2[Cr(D_2O)_6](SO_4)_2$.[23] The warping parameter, β, is similar to previous estimates, ~300 cm^{-1} [18] and 225 cm^{-1}.[22]

The axial (tetragonal) strain, S_θ, was estimated by reproducing the observed Cu−O bond lengths. The magnitude of the deviation of the bond lengths from cubic symmetry is principally determined by $A_1/h\nu_{JT}$. To a good approximation, the axial component of the strain (or the ratio $9\beta/S_\theta$, see refs 19 and 26) determines the bond lengths in the low-temperature limit. The present complexes have almost identical bond lengths at low temperature (Table 1, Figure 2), suggesting that a similar axial strain is present in each lattice. The mean value of $S_\theta \approx -1024$ cm^{-1} is comparable to those values deduced for the $[Cu(H_2O)_6]^{2+}$ ion doped into the host lattices $M_2[Zn(H_2O)_6](SO_4)_2$, where S_θ ranges from −1000 to −550 cm^{-1} for the series M = K, Rb, Cs, and NH_4.[18] (The negative sign indicates that the strain acts as a compression, a common feature of the Tutton salts, which causes the M−O(9) distance to be the shortest bond length, regardless of the transition metal or counterions.)

Within the framework of the RHW model, the parameters S_θ and S_ϵ represent the strain acting on the hypothetical octahedral $[Cu(H_2O)_6]^{2+}$ complex in the absence of vibronic coupling effects. Although in reality these are "effective" parameters, as they are obtained from measurements on the complex after distortion has occurred, similar lattice interactions are expected to be present in the corresponding isomorphous non-JT nickel(II) and zinc(II) complexes. The following equation allows another estimate of S_θ from the

(23) (a) Dobe, C.; Andres, H.-P.; Tregenna-Piggott, P. L. W.; Mossin, S.; Weihe, H.; Janssen, S. *Chem. Phys. Lett.* **2002**, *362*, 387−396. (b) Dobe, C.; Noble, C.; Carver, G.; Tregenna-Piggott, P. L. W.; McIntyre, G. J.; Barra, A.-L.; Neels, A.; Janssen, S.; Juranyi, F. *J. Am. Chem. Soc.* **2004**, *126*, 16639−16652.

(24) Bill, H. In *The Dynamical Jahn−Teller Effect in Localized Systems*; Perlin, Yu. E., Wagner, M., Eds; North-Holland: Amsterdam, 1984; p 791.

(25) (a) Barashkov, M. V.; Zazhogin, A. A.; Komyak, A. I.; Shashkov, S. N. *J. Appl. Spectrosc.* **2000**, *67*, 605−611. (b) Jenkins, T. E.; Lewis, J. *Spectrochim. Acta* **1981**, *37A*, 47−50. (c) Singh, B.; Gupta, S. P.; Khanna, B. N. *Pramana* **1982**, *18*, 427−437. (d) James, D. W.; Whitnall, J. M. *J. Raman Spectrosc.* **1978**, *7*, 225−229. (e) Barashkov, M. V.; Komyak, A. I.; Shashkov, S. N. *J. Appl. Spectrosc.* **2000**, *67*, 216−224. (f) Sekar, G.; Ramakrishnan, V.; Aruldhas, G. *J. Solid State Chem.* **1988**, *74*, 424−427. (g) Choudhury, P.; Ghosh, B.; Patel, M. B.; Bist, H. D. *J. Raman Spectrosc.* **1985**, *16*, 149−155.

(26) Reinen, D.; Krause, S. *Inorg. Chem.* **1981**, *20*, 2750−2759.

M−O bond lengths determined for $K_2[Ni(H_2O)_6](SO_4)_2$ and $K_2[Zn(H_2O)_6](SO_4)_2$[27]

$$S_\theta = 0.1722A_1(d_z - d_o)\sqrt{3}\sqrt{Mh\nu_{JT}} \qquad (6)$$

where $M = 18$ amu (H_2O), $h\nu_{JT} \sim 313$ and 258 cm^{-1} (mean for Ni and Zn Tutton salts, respectively[25]), $A_1 \approx 945$ cm^{-1} (mean, Table 2), and d_z and d_o are the $M-O_{shortest}$ and average M−O bond lengths in Å, respectively. The estimated value for S_θ is ~ -1070 cm^{-1} if the S_θ values of the Ni (~ -900 cm^{-1}) and Zn (~ -1239 cm^{-1}) Tutton salts are averaged, which is consistent with the values listed in Table 2.

The temperature dependence of the long and intermediate bond lengths depends on the energy difference between the two lower minima in the potential surface, and this is decided largely by the orthorhombic component of the strain, S_ϵ.[18,22] The calculated bond length variations giving optimum agreement with experiment in the low-temperature region are shown in Figure 2. The fits are good except for the compounds with 68 and 78% sulfate, where significant deviations occur at higher temperatures: these are discussed in section 3.3. The S_ϵ values producing optimum agreement with the observed bond lengths are given in Table 2. Positive values indicate that the strain corresponds to a relative compression along the Cu−O(7) bonds compared with the Cu−O(8) bonds, while negative ones imply the reverse. It can be seen that the orthorhombic component of the strain decreases in magnitude as the degree of substitution of each counterion increases, and a sign change occurs when selenate is the dominant counterion rather than sulfate.

The most important structural feature associated with the change in sign of S_ϵ is the switch in the long and intermediate Cu−O bond directions, and it is of interest to consider why this should be caused by the replacement of sulfate with selenate. Although the hydrogen bonds to oxygen atoms O(7) and O(8) involved in the switch are quite similar in selenate and sulfate, it does seem that the change in the Cu−O bond lengths is simply accompanied by slight changes in crystal-packing forces because of the difference in the sizes of the counteranions. It should also be noted that the Jahn−Teller radius R_{JT} of the $[Cu(H_2O)_6]^{2+}$ ion, defined as $R_{JT} = [2(d_x)^2 + 2(d_y)^2 + 2(d_z)^2]^{1/2}$, where d_x, d_y, and d_z are the differences in bond lengths from the mean value along each bond direction, is identical within experimental uncertainty in the two forms ($R_{JT} = 0.387$ and 0.389 Å for the pure sulfate and selenate, respectively, at 85 K). This represents a marked difference from $(NH_4)_2[Cu(H_2O)_6](SO_4)_2$ and its deuterated analogue. Here, the deuterated salt in form **A** has a slightly larger distortion than the hydrogenous compound in form **B** ($R_{JT} = 0.377(3)$ Å in the former and 0.332(2) Å in the latter at low temperature), although it is unclear how this is related to the relative stability of the two forms.[4,8,28] It would thus seem that for the sulfate/selenate system, the relative stability of the two forms is the result of general crystal-packing factors and cannot be related to any particular feature. This is in contrast to the $K_2[Cu(H_2O)_6](SeO_4)_2/Rb_2[Cu(H_2O)_6](SeO_4)_2$ system, where the fact that the rubidium salt adopts form **A** may be related to an increase in coordination number of this cation compared with the smaller potassium ion.[29]

Circular cross sections through the lower adiabatic potential surfaces of the $[Cu(H_2O)_6]^{2+}$ ion in the crystal lattices of the pure sulfate and selenate and the mixed crystals with 68 and 25% sulfate at the Jahn−Teller radius ρ_o calculated

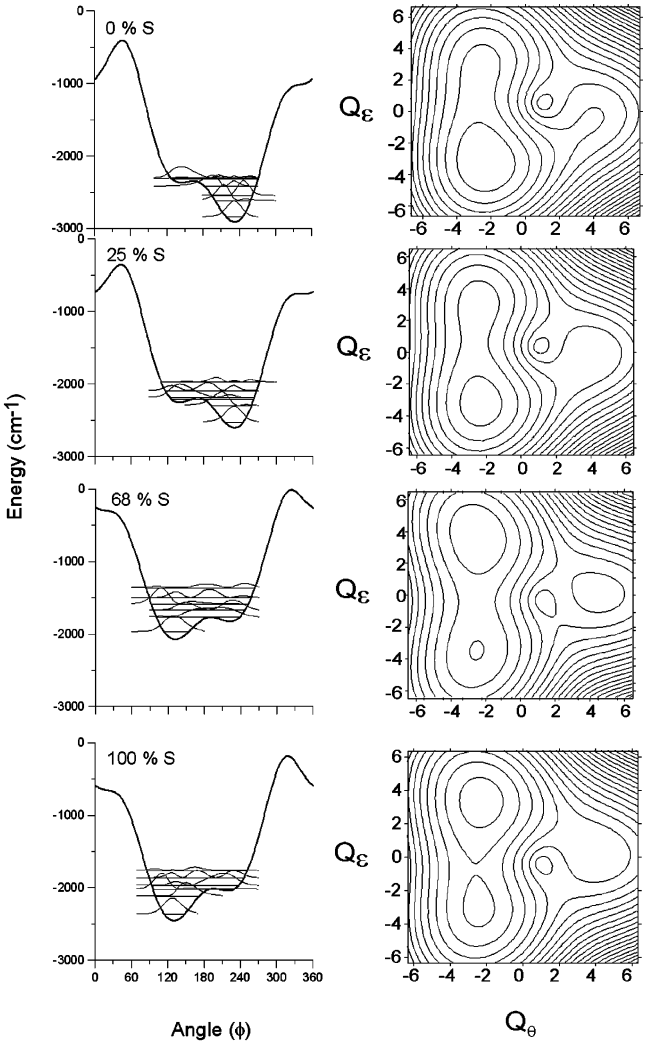

Figure 3. (left) Variation of the energy of the potential surface of the $[Cu(H_2O)_6]^{2+}$ ion in several lattices plotted as a function of the relative displacement along the components of the Jahn−Teller e_g vibration at the radius of the Jahn−Teller minimum, ρ_o, calculated with eq 2 and the parameters in Table 2. The transformation from R_{JT} (Å) to ρ_o (dimensionless) follows from eq 4: $\rho_o = R_{JT}(Mh\nu_{JT})^{1/2}/5.806$. The squares of the vibrational components of the six lowest vibronic wave functions are also shown. (right) Contour energy plots of the lower region of the potential surface given by eq 2. It should be noted that the path of least energy around the potential is far from circular, being a function of both ρ_o and ϕ, as shown in the two-dimensional contour plots.

(27) d(Ni−O) = 2.0761(9), 2.0837(8), 2.0203(9) Å (T = 296 K); 2.0760(7), 2.0830(7), 2.0155(7) Å (T = 200 K); 2.0763(7), 2.0852(6), 2.0130(7) Å (T = 95 K) for Ni−O(7), Ni−O(8), and Ni−O(9), respectively, in $K_2[Ni(H_2O)_6](SO_4)_2$. d(Zn−O) = 2.1263(7), 2.1336(7), 2.0342(8) Å (T = 296 K); 2.1247(9), 2.1319(9), 2.0329(9) Å (T = 296 K); 2.1247(8), 2.1311(8), 2.0334(9) Å (T = 296 K); 2.1241(7), 2.1326(7), 2.0333(7) Å (T = 260 K); 2.1224(6), 2.1336(6), 2.0287(6) Å (T = 120 K); 2.1222(6), 2.1336(6), 2.0275(6) Å (T = 95 K) for Zn−O(7), Zn−O(8), and Zn−O(9), respectively, in $K_2[Zn(H_2O)_6](SO_4)_2$. Simmons, C. J.; Stratemeier, H.; Hitchman, M. A. Unpublished results.

(28) Figgis, B. N.; Sobolev, A. N.; Simmons, C. J.; Hitchman, M. A.; Stratemeier, H.; Riley, M. J. *Acta Crystallogr.* **2000**, *B56*, 438−443.

(29) Simmons, C. J.; Stratemeier, H.; Hitchman, M. A. Unpublished results.

Table 3. Calculated Bond Lengths of the Six Lowest Vibronic Energy Levels for $K_2[Cu(H_2O)_6](SO_4)_{2x}(SeO_4)_{2-2x}$

100 % SO_4				0% SO_4			
energy (cm^{-1})	Cu−O(8)	Cu−O(7)	Cu−O(9)	energy (cm^{-1})	Cu−O(7)	Cu−O(8)	Cu−O9
0	2.265	2.051	1.965	0	2.309	2.034	1.944
246	2.246	2.074	1.961	228	2.298	2.049	1.941
344	2.265	2.048	1.968	294	2.310	2.031	1.947
455[a]	2.157	2.166	1.957	425	2.269	2.083	1.936
396							
501	2.179	2.141	1.960	525	2.285	2.060	1.943
600	2.249	2.068	1.963	543[a]	2.181	2.174	1.933
				538			
78% SO_4				17% SO_4			
energy (cm^{-1})	Cu−O(8)	Cu−O(7)	Cu−O(9)	energy (cm^{-1})	Cu−O(7)	Cu−O(8)	Cu−O9
0	2.247	2.065	1.969	0	2.287	2.043	1.951
230	2.206	2.110	1.966	231	2.271	2.063	1.947
341[a]	2.150	2.166	1.966	314	2.287	2.040	1.954
336							
374	2.247	2.063	1.972	394	2.182	2.158	1.941
486	2.175	2.140	1.966	470[a]	2.176	2.160	1.944
				467			
617	2.212	2.102	1.967	552	2.273	2.058	1.949
68% SO_4				25% SO_4			
energy (cm^{-1})	Cu−O(8)	Cu−O(7)	Cu−O(9)	energy (cm^{-1})	Cu−O(7)	Cu−O(8)	Cu−O9
0	2.309	2.029	1.939	0	2.280	2.049	1.951
268[a]	2.296	2.041	1.939	224	2.259	2.075	1.947
235							
311	2.061	2.278	1.937	320	2.281	2.046	1.954
321	2.304	2.031	1.941	405[a]	2.137	2.201	1.943
				341			
449	2.239	2.098	1.939	431	2.193	2.142	1.946
517	2.122	2.216	1.938	552	2.257	2.075	1.949

[a] Energy calculated using the Silver and Getz model (see Figure 4).

using eq 2 and the optimum values in Table 2 are shown in Figure 3, along with the corresponding contour energy plots. The relationship between ρ_o (dimensionless) and R_{JT} (Å) follows from eq 4: $\rho_o = R_{JT}(Mh\nu_{JT})^{1/2}/5.806$. A sectional plot of the square of the vibrational part of the wave function associated with the six lowest levels is also shown on each plot. The most obvious feature for the present compounds is the fact that the lowest minimum occurs close to 120° when the dominant counterion is sulfate and 240° when it is selenate. These angles correspond to tetragonal elongations with the long axes along *x* and *y*, respectively. (Note that the direction of the axial compression, which is associated with the shortest Cu−O bond, is defined as the *z* axis.[18]) The bond lengths associated with the six lowest vibronic states of each compound are given in Table 3. The calculated overall bond lengths are compared with those observed experimentally for each compound as a function of temperature in Figure 2. Finally, it should be noted that the axial strain is the dominant factor influencing the energy of the highest of the three mimina in the ground-state surface. The energy difference between highest- and lowest-energy minima, ~1900 cm^{-1}, is consistent with the fact that the Cu−O(9) bond lengths are temperature independent up to $T = 320$ K.

For the pure sulfate and selenate, the second-lowest minimum of the potential surface is rather shallow, and the vibronic wave functions lying just above it are quite delocalized (Figure 3). As may be seen from Table 3, for

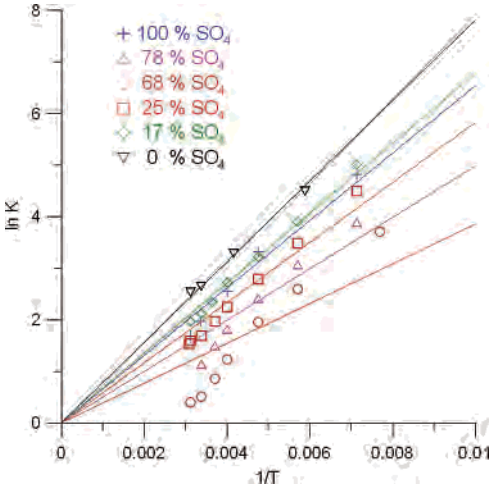

Figure 4. Plots showing the dependence of *K*, the ratio of the complexes in the lower energy well (N_1) to those in the upper energy well (N_2), on the temperature. The lines represent "best-fits" assuming a linear relationship between ln *K* and 1/*T*.

these compounds there is no single energy level corresponding to a tetragonally elongated geometry with the direction of the long axis switched compared with that of the lowest level. Instead, two levels with bonds along *x* and *y* approximately equal in length occur for the pure sulfate at 396 and 501 cm^{-1}. This situation has been observed for other compounds[18,20,22] and occurs when the orthorhombic component of the strain is comparable in magnitude to the parameter β representing the higher-order warping effects of the Mexican hat potential surface. Although thermal occupancy of these two upper levels has a similar effect to the population of a single level with the bond lengths along *x* and *y* interchanged, these compounds formally deviate from this simplistic assumption of the SG model, although the mean energy of these two upper levels, 449 cm^{-1}, is very close to $E_{SG} = 455$ cm^{-1}. As may be seen from Figure 3, the second minimum is better defined for the potential surface of the $[Cu(H_2O)_6]^{2+}$ ions in the compound with 68% sulfate. This is because the orthorhombic strain is considerably smaller than in the pure salts. For this compound, the bond lengths associated with the wave function just above the second minimum (second excited vibronic level) correspond well to a geometry like that of the lowest wave function, but with the *x* and *y* components interchanged (Table 3), so that the SG model is obeyed (311 cm^{-1} vs $E_{SG} = 268$ cm^{-1}).

Even though the wave functions imply that the underlying assumptions of Silver and Getz do not always hold, a satisfactory fit to the experimental data in the low-temperature region may be obtained for most of the compounds using their model as shown in the plots presented in Figure 4. Their model, as implemented by Simmons[30,31] for bond lengths, assumes that the observed Cu−O bond lengths are the weighted averages of two potential wells of the warped Mexican-hat surface. (Because the Cu−O(9) bond lengths are temperature independent, the third well is much too high

(30) Simmons, C. J.; Hathaway, B. J.; Amornjarusiri, K.; Santarsiero, B. D.; Clearfield, A. *J. Am. Chem. Soc.* **1987**, 1947−1958.
(31) Simmons, C. J. *New J. Chem.* **1993**, *17*, 77−95.

in energy to be appreciably populated.) When the fractional populations of the wells are N_1 and N_2 ($N_1 + N_2 = 1$), the observed Cu−O bond lengths at a particular temperature are

$$d(\mathrm{Cu-O(7)})_{\mathrm{obsd}} = N_1 d(\mathrm{Cu-O(7)^l})_{1,\mathrm{static}} + N_2 d(\mathrm{Cu-O(7)^i})_{2,\mathrm{static}} \quad (7a)$$

$$d(\mathrm{Cu-O(8)})_{\mathrm{obsd}} = N_1 d(\mathrm{Cu-O(8)^i})_{1,\mathrm{static}} + N_2 d(\mathrm{Cu-O(8)^l})_{2,\mathrm{static}} \quad (7b)$$

$$d(\mathrm{Cu-O(9)})_{\mathrm{obsd}} = N_1 d(\mathrm{Cu-O(9)^s})_{1,\mathrm{static}} + N_2 d(\mathrm{Cu-O(9)^s})_{2,\mathrm{static}} \quad (7c)$$

where $N_1 = Z$, $N_2 = Z\exp(-\delta_{12}/kT)$, $Z = [1 + \exp(-\delta_{12}/kT)]^{-1}$, δ_{12} is the energy difference between the two lowest-energy wells, $d(\mathrm{Cu-O(7)^l})_{1,\mathrm{static}}$ is the long Cu−O(7) bond length in well 1, $d(\mathrm{Cu-O(7)^i})_{2,\mathrm{static}}$ is the intermediate Cu−O(7) bond length in well 2, etc., and $d(\mathrm{Cu-O(7)})_{\mathrm{obsd}} > d(\mathrm{Cu-O(8)})_{\mathrm{obsd}} > d(\mathrm{Cu-O(9)})_{\mathrm{obsd}}$. It is assumed that the Cu−O bond lengths are identical in all isomers, that reorientations result in an interchange of the *x*, *y*, and *z* axes only,[32] and that δ_{12} is temperature independent. $\delta_{12} = E_{\mathrm{SG}}$ is varied using the d(Cu−O(7)) and d(Cu−O(8)) static bond lengths at 85 K (Table 1) to get the best least-squares fit between observed and calculated bond lengths. E_{SG} is equal to the slope of a least-squares plot of ln K versus $1/T$, where $K = N_1/N_2$. Linear behavior is observed for the present compounds, though significant deviations occur at higher temperatures for the compounds with 68 and 78% sulfate; these will be discussed in the following section. The estimates of E_{SG} for the present compounds are listed in Table 3. As discussed previously, the Silver−Getz energy corresponds approximately with either the energy of the vibronic wave function having bond length displacements in which the intermediate and long bonds are exchanged compared to those in the ground state or with the energies of two delocalized wave functions.

The relative slopes of the ln K versus $1/T$ plots in Figure 4 reveal how the magnitude of the orthorhombic strain of the pure selenate compound decreases as sulfate is added, reaching the lowest value at 68% sulfate and then increasing for 78 and 100% sulfate. This effect can also be seen in Figure 5, where a plot of the difference in the mean-square displacement amplitudes along the Cu−O bonds, ΔU_{obsd}(Cu−O), as a function of sulfate composition is shown. The values of ΔU_{obsd}(Cu−O(7)) and ΔU_{obsd}(Cu−O(8)) are clearly much larger for the compound with 68% sulfate, interpolating to a value of ca. 0.022 Å^2 for a hypothetical $K_2[Cu(H_2O)_6](SO_4)_{2x}(SeO_4)_{2-2x}$ compound containing ~50% sulfate (vide infra). As the magnitude of the orthorhombic strain diminishes, the thermal population of the higher of the two lower-energy minima increases and the complex exhibits a greater degree of fluxionality and disorder, as revealed by the larger ΔU_{obsd}(Cu−O) values.

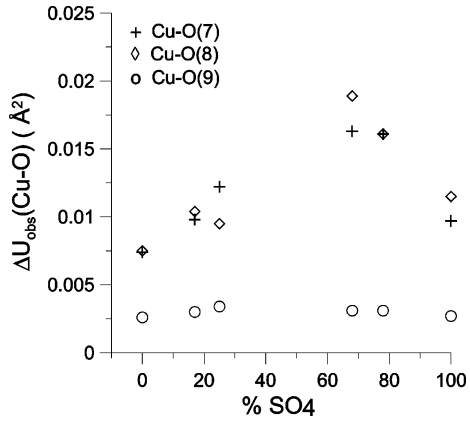

Figure 5. Plots of the difference in the mean-square displacement amplitudes along Cu−O bonds, ΔU_{obsd}(Cu−O), as a function of sulfate composition at 298 K. The corresponding ΔU_{obsd}(M−O) values for the isomorphous non-Jahn−Teller complexes, $K_2[Ni(H_2O)_6](SO_4)_2$ and $K_2[Zn(H_2O)_6](SO_4)_2$, are 0.0024 and 0.0015 Å^2, respectively. The estimated maximum value for a hypothetical $K_2[Cu(H_2O)_6](SO_4)_{2x}(SeO_4)_{2-2x}$ compound containing 50% sulfate is ~0.022 Å^2 (see text for details).

Stebler and Bürgi[34] have, in effect, shown how ΔU_{obsd}'s can be calculated for a Jahn−Teller molecule that essentially obeys the SG model. In the present case, the ΔU's may also contain contributions from a not entirely homogeneous distribution of the selenate anions in the sulfate lattice (and vice versa). Thus, the polyhedron geometry may differ slightly in a mixed crystal depending on the specific anion second-sphere environment. As discussed above, for most of the present compounds, the RHW approach suggests that the upper states involved in the thermal equilibrium do not approximate well to the SG model, being quite delocalized. However, except for the deviations considered in the following section, the bond length changes behave in the manner suggested by the SG approach, so, while the above limitations must be kept in mind, the Stebler−Bürgi procedure is followed here. Accordingly, it is assumed that $d(\mathrm{Cu-O(7)^l})_{1,\mathrm{static}} = d(\mathrm{Cu-O(8)^l})_{2,\mathrm{static}}$, $d(\mathrm{Cu-O(8)^i})_{1,\mathrm{static}} = d(\mathrm{Cu-O(7)^i})_{2,\mathrm{static}}$, and $d(\mathrm{Cu-O(9)^s})_{1,\mathrm{static}} = d(\mathrm{Cu-O(9)^s})_{2,\mathrm{static}}$. The ΔU_{obsd}'s can be calculated by summing the contributions from the internal stretching motions not related to the JT deformation and the contributions from the static JT distortions. One then finds that ΔU_{obsd} for the Cu−O(7) and Cu−O(8) bonds is given by the following[17,34]

$$\Delta U_{\mathrm{obsd}} = a_{\mathrm{o}} + a_1\langle \Delta d(\mathrm{Cu-O})\rangle - \langle \Delta d(\mathrm{Cu-O})\rangle^2 \quad (8)$$

where $a_{\mathrm{o}} = (\Delta U_1 + \Delta U_i)/2 + [\Delta d(\mathrm{Cu-O})]^2$ and $a_1 = (\Delta U_l - \Delta U_i)/2\Delta d(\mathrm{Cu-O})$. Here $\Delta d(\mathrm{Cu-O}) \equiv [d(\mathrm{Cu-O(7)^l})_{1,\mathrm{static}} - d(\mathrm{Cu-O(7)^i})_{2,\mathrm{static}}]/2 = [d(\mathrm{Cu-O(8)^l})_{2,\mathrm{static}} - d(\mathrm{Cu-O(8)^i})_{1,\mathrm{static}}]/2 = [d(\mathrm{Cu-O(7)^l})_{1,\mathrm{static}} - d(\mathrm{Cu-O(8)^i})_{1,\mathrm{static}}]/2 = [d(\mathrm{Cu-O(8)^l})_{2,\mathrm{static}} - d(\mathrm{Cu-O(7)^i})_{2,\mathrm{static}}]/2$ or half the difference in the actual (static), long, and intermediate bond lengths, $\langle \Delta d(\mathrm{Cu-O})\rangle \equiv [\langle d(\mathrm{Cu-O(8)})\rangle - \langle d(\mathrm{Cu-O(7)})\rangle]/$

(32) That the *g* values (or bond lengths) in the higher-energy well can differ from those in the lowest well has been indicated by theoretical calculations,[18] EPR spectra of mixed Tutton salts,[33] and the crystal structure of $[Cu(phen)_2(CH_3CO_2)](ClO_4)_2$, where the Cu−O bond lengths of the structures associated with the two wells are noticeably different.[31]

(33) Augustyniak-Jablokow, M. A. *J. Phys. Chem. Solids* **2001**, *62*, 1319; Augustyniak-Jablokow, M. A.; Krupska, A.; Krupski, M.; Yablokov, Y. V. *Inorg. Chem.* **2002**, *41*, 1348.

(34) Stebler, M.; Bürgi, H. B. *J. Am. Chem. Soc.* **1987**, *109*, 1395−1401.

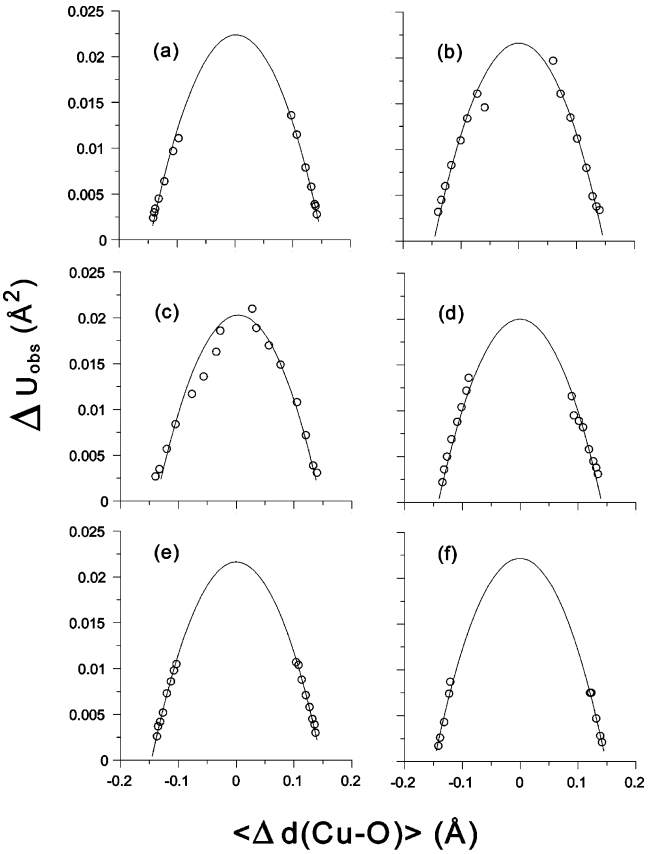

Figure 6. Scatter plots of ΔU_{obsd}(Cu−O) (Å^2) vs $\langle\Delta d$(Cu−O)$\rangle$ (Å) for (a) 100, (b) 78, (c) 68, (d) 25, (e) 17, and (f) 0% sulfate. The solid lines represent the quadratic fits of eq 8, $\Delta U_{obsd} = a_o + a_1\langle\Delta d(\text{Cu}-\text{O})\rangle - \langle\Delta d(\text{Cu}-\text{O})\rangle^2$, with the following values: $a_o = 0.0224$ Å^2, $a_1 = 0.0045$ Å (100% sulfate); $a_o = 0.0216$ Å^2, $a_1 = 0.0005$ Å (78% sulfate); $a_o = 0.0203$ Å^2, $a_1 = 0.0077$ Å (68% sulfate); $a_o = 0.0200$ Å^2, $a_1 = 0.0$ Å (25% sulfate); $a_o = 0.0216$ Å^2, $a_1 = 0.0012$ Å (17% sulfate); $a_o = 0.0222$ Å^2, $a_1 = 0.0$ Å (0% sulfate).

2, or half the difference in the observed bond lengths, and ΔU_l and ΔU_i are contributions from internal stretching motions unrelated to the Jahn−Teller distortion. This equation predicts that there will be a quadratic dependence of the ΔU_{obsd}'s on half the difference in the observed bond lengths, $\langle\Delta d$(Cu−O)$\rangle$, that $\Delta U_{obsd}(\text{max}) = a_o + a_1^2/4$, and that the maximum value of $\langle\Delta d$(Cu−O)$\rangle$ occurs at $a_1/2 \sim 0$.

The anisotropic displacement parameters given in Supporting Information Table 3 allow ΔU_{obsd} values to be calculated for all compounds; they are plotted against $\langle\Delta d$(Cu−O)$\rangle$ in Figure 6. A structure determination of a compound at a given temperature contributes two points: ΔU_{obsd}(Cu−(O7)) at negative $\langle\Delta d$(Cu−O)$\rangle$ and ΔU_{obsd}(Cu−O(8)) at positive $\langle\Delta d$(Cu−O)$\rangle$. The coefficients of the quadratic term have been constrained to −1 to conform with the equation. In general, there is very good agreement with the predicted quadratic dependence of eq 8. Since $a_o \sim 0.022$ Å^2 and $a_1 \sim 0$, $\Delta U_{obsd}(\text{max}) \sim 0.022$ Å^2, nearly identical to the value of 0.021 Å^2 reported for a similar study of $(ND_4)_2[Cu(D_2O)_6](SO_4)_2$ and $(NH_4)_2[Cu(H_2O)_6](SO_4)_2$.[17] If we assume that $\Delta U_1 = \Delta U_i = \Delta U$, then $a_1 = 0$ and $a_o = \Delta U + [\Delta d(\text{Cu}-\text{O})]^2$. One can estimate the value of ΔU from the temperature-independent ΔU(Cu−O(9)) as ∼0.002 Å^2 and use $a_o = 0.022$ Å^2; thus, Δd(Cu−O) ∼ 0.141 Å or $|d(\text{Cu}-\text{O}(8)) - d(\text{Cu}-\text{O}(7))|_{max} \sim 0.282$ Å. An inspection of the observed bond lengths at 85 K in Table 1 indicates excellent agreement with the estimated value. Collectively, these results indicate that at all temperatures and for all compounds the averaging of the bond lengths can be considered, in an approximate sense, as a thermal equilibrium between two Jahn−Teller isomers, as assumed by the both the Silver−Getz and Stebler−Bürgi models.

3.3. Cooperative Model of Vibronic Interactions. As stated previously, the experimental points in the higher-temperature region deviate significantly from the linear dependence predicted by the SG model for compounds with 68 and 78% sulfate (Figure 4). A similar discrepancy occurs for the plots derived from the RHW model (Figure 2). This behavior is very similar to that observed for the M−O bond lengths of $(NH_4)_2[Cu(H_2O)_6](SO_4)_2$ and its deuterated analogue,[7] $(ND_4)_2[Cr(D_2O)_6](SO_4)_2$[23], and the g values of $Cs_2\{Zn[Cu](H_2O)_6\}(ZrF_6)_2$.[22] For $(ND_4)_2[Cu(D_2O)_6](SO_4)_2$, satisfactory agreement with experiment was obtained using an approach analogous to the SG model but extended to include cooperative interactions between neighboring complexes.[7] Basically, the cooperative model assumes that the change in geometry induced by thermal excitation of one complex alters the lattice strain acting on its neighbors. Agreement with the experiment was obtained if just the orthorhombic component of the strain is affected, and this influences just the four nearest neighbors in the *xy* plane. Such behavior is consistent with the crystal packing in the Tutton salts, since the $[Cu(H_2O)_6]^{2+}$ ions are stacked in the common antiferrodistortive manner,[35] with the short Cu−O bonds of all complexes parallel and the long and intermediate bonds of neighboring complexes approximately parallel.

The cooperative model also gives a satisfactory fit to the experimental data of the mixed sulfate/selenate salts (Figure 7) using the values of the basic lattice interaction energy, E, and cooperative interaction energy, J_{xy}, given in Table 4. Here, the optimum values were obtained by comparing the calculated and observed bond lengths at each temperature for all reasonable combinations of E and J_{xy}. Because of the random statistics involved in the modeling,[7] the calculation for each combination does not produce a unique result, and this was taken into account by averaging the results of hundreds of calculations. Each optimum value in Table 4 is that giving the smallest difference between the calculated and observed bond lengths, the standard deviation being estimated by standard statistical methods.[36]

As discussed in detail previously,[7] E represents the underlying lattice strain which is independent of the orientation of neighboring complexes, while J describes the interaction from each neighboring complex, this being negative when the complex is in its ground state and positive when it is in the excited state. In the present case, the cooperative interaction with complexes along z, the direction of the short Cu−O bonds, J_z, may be ignored, as these bond

(35) Bersuker, I. B. *The Jahn−Teller Effect and Vibronic Interactions in Modern Chemistry*; Plenum: New York, 1984.
(36) The least-squares method used to treat the data was taken from the following Internet site: www.beyondtechnology.com/tipsO16.shtml.

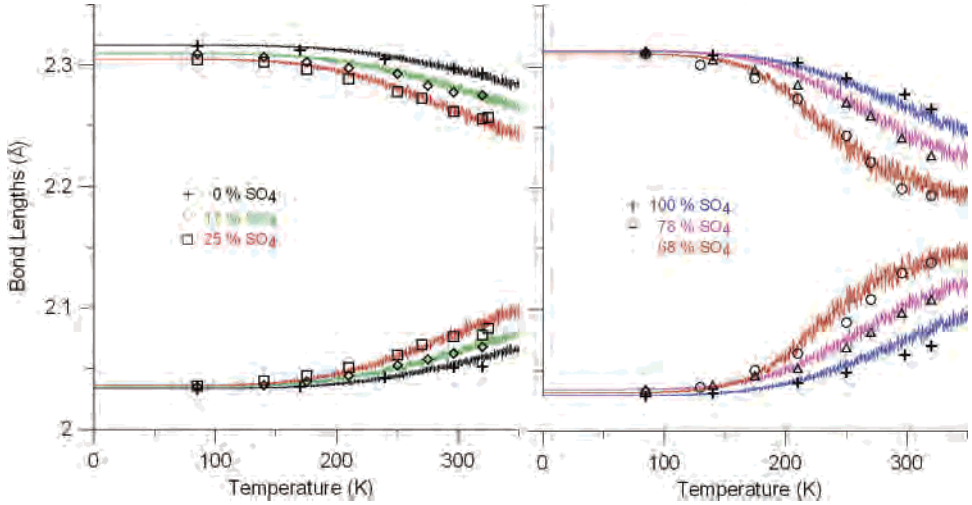

Figure 7. Temperature dependence of the bond lengths calculated assuming cooperative interactions between complexes compared with the experimental values; see Table 4 for the values of the cooperative coupling constant J_{xy} and basic lattice strain energy E.

Table 4. Lattice Strain Energies, E, and Cooperative Interaction Energies, J_{xy}, for $K_2[Cu(H_2O)_6](SO_4)_{2x}(SeO_4)_{2-2x}$

% SO_4	0	17	25	68	78	100
E (cm^{-1})	231(14)	192(6)	116(5)	30(4)	100(9)	159(5)
J_{xy} (cm^{-1})	49(2)	43(1)	49(2)	52(2)	41(2)	46(1)

lengths are unaffected by temperature. As in previous treatments,[7] the calculation makes the approximation that the cooperative interactions between neighbors along the x and y directions are equivalent. As noted above, in most of the present cases the excited-state geometry does not conform to the predictions of the SG model. However, the change in geometry on excitation follows a pattern similar to that predicted by this model (Table 3), so it is likely that the cooperative interactions will act in a similar manner. At low temperature, the energy of every complex is therefore $-4J_{xy}$ with an excited-state energy of $E + 4J_{xy}$. For a complex with one neighbor in the excited state, the ground-state energy is $-2J_{xy}$ and the excited-state energy is $E + 2J_{xy}$, while for a complex with two neighbors in the upper state, the energy of the excited-state energy is just E. The average energy of excitation for the lattice thus falls as the temperature and the number of complexes in the upper state increases. This is the reason some of the plots in Figure 4 deviate significantly from linearity at smaller values of $1/T$ (i.e., at higher temperatures).

A comparison of the parameters in Table 4 shows that the underlying lattice interaction energy is generally larger than the cooperative interaction between two complexes. However, while the nature of the counterion strongly influences E, it has little effect on the cooperative interaction. This seems reasonable. While the lattice perturbation on the $[Cu(H_2O)_6]^{2+}$ ion is expected to be quite sensitive to the details of its surroundings, the cooperative interaction depends on the separation and disposition of neighboring complexes; this does not change much when sulfate is replaced by selenate. The pure selenate has a stronger lattice interaction than the pure sulfate, with E decreasing progressively as each anion is replaced by the other. These trends mirror exactly those of the orthorhombic strain interaction inferred using the RHW model (Table 2) and the energy separation of the structural isomers deduced using the SG model (Table 3). The energy to excite a complex when all its neighbors are in the ground state ($E + 8J_{xy}$) is generally quite similar to the energy difference deduced using the SG model and given in Table 3.

It is apparent that significant deviations from Boltzmann behavior occur only for the salts with 68 and 78% sulfate at higher temperatures (Figures 2 and 4). This is because such deviations are expected only when the proportion of complexes in the excited state is large enough to make it probable that excitation will occur to a neighbor. It is only for these two mixed salts that the excitation energy is so small that this occurs at a low enough temperature to be observed. From the temperature dependence of the bond lengths, it can be seen that deviations occur at ~200 K for the former and ~230 K for the latter salt. In both cases, this corresponds to ~20% of the complexes being in the excited state, so this is presumably the concentration at which the cooperative interactions make it likely that excitation will occur at neighboring sites. The higher excitation energies of the pure compounds and other mixed-anion salts mean that this concentration is not reached by the highest temperature at which the compounds remain stable, 320 K.

The results in Table 4 may be compared with the values of $E = 9$ and $J_{xy} = 76.5$ cm^{-1} deduced for $(ND_4)_2[Cu(D_2O)_6](SO_4)_2$.[7] The basic pattern is similar, as expected, given the similarity of the structures. However, the underlying strains are larger and the cooperative interactions smaller for the present compounds. Such differences are not unexpected, as the cooperative interactions are presumably transmitted via the hydrogen-bonding network, and this involves the cation in the ammonium but not the potassium salt. The present results are important in this context, since it has been proposed that onset of rotations of the ammonium groups at higher temperatures may influence the thermal behavior of the deuterated ammonium complex.[1,37] This cannot, of

(37) Augustyniak, M. A.; Usachev, A. E. *J. Phys.: Condens. Matter* **1999**, *11*, 4391−4400.

course, occur for the present complexes, strengthening the idea that cooperative interactions are indeed the cause of the anomalous thermal behavior at higher temperatures.

If cooperative interactions indeed play a significant role in the lattice interactions of these copper(II) compounds, the influence of these upon the potential surfaces derived by the RHW model should be considered. It must be recognized that the strain parameters used to derive the potential surfaces involve all lattice interactions, including those from the neighboring complexes. The potential surfaces derived for the present complexes are quite valid as long as it is recognized that they refer only to complexes surrounded by neighbors in their ground states. Complexes with one or two neighbors with orientations corresponding to the excited state will have different potential surfaces with much smaller energy differences between the two lowest minima. In principle, these potential surfaces could be calculated by appropriately modifying the orthorhombic strain parameter, S_ϵ.

4. Conclusions

The long and intermediate bonds of the Jahn−Teller distorted $[Cu(H_2O)]_6^{2+}$ ion in the mixed-anion salt $K_2[Cu(H_2O)_6](SO_4)_{2x}(SeO_4)_{2-2x}$ switch direction between 25 and 68% sulfate. A thermal equilibrium is observed between these two forms, with this developing more readily as the proportion of the two anions becomes more similar. The temperature dependence of the Cu−O bond lengths may be interpreted satisfactorily by calculating the Jahn−Teller potential surface of the $[Cu(H_2O)_6]^{2+}$ ion under the influence of a lattice strain used to quantify the low site symmetry. When the orthorhombic component of this strain is small, cooperative interactions between neighboring complexes influence the behavior at higher temperatures.

Acknowledgment. Financial assistance from the Australian Research Commission is acknowledged by M.A.H. and H.S. We are also grateful for a reviewer's insightful comments concerning the models that we use to interpret our data.

Supporting Information Available: Additional tables and crystallographic data in CIF format. This material is available free of charge via the Internet at http://pubs.acs.org.

IC050790J